The Astrophysical Journal Letters, 955:L2 (8pp), 2023 September 20 https://doi.org/10.3847/2041-8213/acf57c
© 2023. The Author(s). Published by the American Astronomical Society.
OPEN ACCESS

Reionization and the ISM/Stellar Origins with JWST and ALMA (RIOJA): The Core of the Highest-redshift Galaxy Overdensity at $z = 7.88$ Confirmed by NIRSpec/JWST

T. Hashimoto[1,2], J. Álvarez-Márquez[3], Y. Fudamoto[4,5], L. Colina[3], A. K. Inoue[4,6], Y. Nakazato[7], D. Ceverino[8,9], N. Yoshida[7,10,11], L. Costantin[3], Y. Sugahara[4,5], A. Crespo Gómez[3], C. Blanco-Prieto[3], K. Mawatari[1,2], S. Arribas[3], R. Marques-Chaves[12], M. Pereira-Santaella[13], T. J. L. C. Bakx[5,14], M. Hagimoto[14], T. Hashigaya[15], H. Matsuo[16,17], Y. Tamura[14], M. Usui[1], and Y. W. Ren[18]

[1] Division of Physics, Faculty of Pure and Applied Sciences, University of Tsukuba, Tsukuba, Ibaraki 305-8571, Japan; hashimoto.takuya.ga@u.tsukuba.ac.jp
[2] Tomonaga Center for the History of the Universe (TCHoU), Faculty of Pure and Applied Sciences, University of Tsukuba, Tsukuba, Ibaraki 305-8571, Japan
[3] Centro de Astrobiología (CAB), CSIC-INTA, Ctra. de Ajalvir km 4, Torrejón de Ardoz, E-28850 Madrid, Spain
[4] Waseda Research Institute for Science and Engineering, Faculty of Science and Engineering, Waseda University, 3-4-1 Okubo, Shinjuku, Tokyo 169-8555, Japan
[5] National Astronomical Observatory of Japan, 2-21-1, Osawa, Mitaka, Tokyo, Japan
[6] Department of Physics, School of Advanced Science and Engineering, Faculty of Science and Engineering, Waseda University, 3-4-1, Okubo, Shinjuku, Tokyo 169-8555, Japan
[7] Department of Physics, The University of Tokyo, 7-3-1 Hongo, Bunkyo, Tokyo 113-0033, Japan
[8] Universidad Autonoma de Madrid, Ciudad Universitaria de Cantoblanco, E-28049 Madrid, Spain
[9] CIAFF, Facultad de Ciencias, Universidad Autonoma de Madrid, E-28049 Madrid, Spain
[10] Kavli Institute for the Physics and Mathematics of the Universe (WPI), UT Institute for Advanced Study, The University of Tokyo, Kashiwa, Chiba 277-8583, Japan
[11] Research Center for the Early Universe, School of Science, The University of Tokyo, 7-3-1 Hongo, Bunkyo, Tokyo 113-0033, Japan
[12] Geneva Observatory, Department of Astronomy, University of Geneva, Chemin Pegasi 51, CH-1290 Versoix, Switzerland
[13] Instituto de Física Fundamental (IFF), CSIC, Serrano 123, E-28006 Madrid, Spain
[14] Department of Physics, Graduate School of Science, Nagoya University, Nagoya 464-8602, Japan
[15] Department of Astronomy, Kyoto University Sakyo-ku, Kyoto 606-8502, Japan
[16] National Astronomical Observatory of Japan, 2-21-1 Osawa, Mitaka, Tokyo 181-8588, Japan
[17] Graduate University for Advanced Studies (SOKENDAI), 2-21-1 Osawa, Mitaka, Tokyo 181-8588, Japan
[18] Department of Pure and Applied Physics, Graduate School of Advanced Science and Engineering, Faculty of Science and Engineering, Waseda University, 3-4-1 Okubo, Shinjuku, Tokyo 169-8555, Japan

Received 2023 May 8; revised 2023 August 17; accepted 2023 August 30; published 2023 September 13

Abstract

The protoclusters in the epoch of reionization, traced by galaxy overdensity regions, are ideal laboratories for studying the process of stellar assembly and cosmic reionization. We present the spectroscopic confirmation of the core of the most distant protocluster at $z = 7.88$, A2744-z7p9OD, with the James Webb Space Telescope NIRSpec integral field unit spectroscopy. The core region includes as many as four galaxies detected in [O III] 4960 and 5008 Å in a small area of $\sim 3'' \times 3''$, corresponding to $\sim 11 \times 11$ kpc, after the lensing magnification correction. Three member galaxies are also tentatively detected in dust continuum in Atacama Large Millimeter/submillimeter Array Band 6, which is consistent with their red ultraviolet continuum slopes, $\beta \sim -1.3$. The member galaxies have stellar masses in the range of $\log(M_*/M_\odot) \sim 7.6$–$9.2$ and star formation rates of $\sim$3–50 $M_\odot$ yr^{-1}, showing a diversity in their properties. FirstLight cosmological simulations reproduce the physical properties of the member galaxies including the stellar mass, [O III] luminosity, and dust-to-stellar mass ratio, and predict that the member galaxies are on the verge of merging in a few to several tens of Myr to become a large galaxy with $M_* \sim 6 \times 10^9 M_\odot$. The presence of a multiple merger and evolved galaxies in the core region of A2744-z7p9OD indicates that environmental effects are already at work 650 Myr after the Big Bang.

Unified Astronomy Thesaurus concepts: Primordial galaxies (1293); Protoclusters (1297)

1. Introduction

Understanding the properties of galaxies at redshift of $z \gtrsim 6$ is crucial for studying galaxy formation and evolution as well as the process of cosmic reionization. With the advent of the James Webb Space Telescope (JWST; Gardner et al. 2023), it has become possible to study detailed properties of high-redshift galaxies (e.g., Curtis-Lake et al. 2023; Bunker et al. 2023).

The overdense regions of galaxies, protoclusters, offer us the opportunity to study environmental effects of galaxy formation (e.g., Dressler 1980; Koyama et al. 2008). Protoclusters in the epoch of reionization (EoR) are interesting because they probe early galaxy formation and stellar mass assembly.

An interesting candidate protocluster, A2744-z7p9OD, at $z \approx 7$–8 behind the strong lensing cluster Abell 2744 was reported based on photometric redshift deduced from HST data taken as a part of Hubble Frontier Fields Survey (PI: Lotz) in conjunction with Spitzer/IRAC data (Laporte et al. 2014; Zheng et al. 2014; Ishigaki et al. 2016). The protocluster includes 11 member galaxy candidates at $7 < z < 8$ labeled as A2744-ZD1, ZD2, ..., ZD11 and 11 candidates at $8 < z < 9$ labeled as A2744-YD1, YD2, ..., YD11 within a single field of view of HST WFC3. Among these, particularly interesting is the "quintet" galaxies at $z \sim 8$ (YD1, YD4, YD6, YD7, and ZD1) in a distance of $\sim 3'' \times 3''$, as shown in the left panel of Figure 1.

Recently, Morishita et al. (2023) have reported the spectroscopic redshift of A2744-z7p9OD by identifying seven

Original content from this work may be used under the terms of the Creative Commons Attribution 4.0 licence. Any further distribution of this work must maintain attribution to the author(s) and the title of the work, journal citation and DOI.

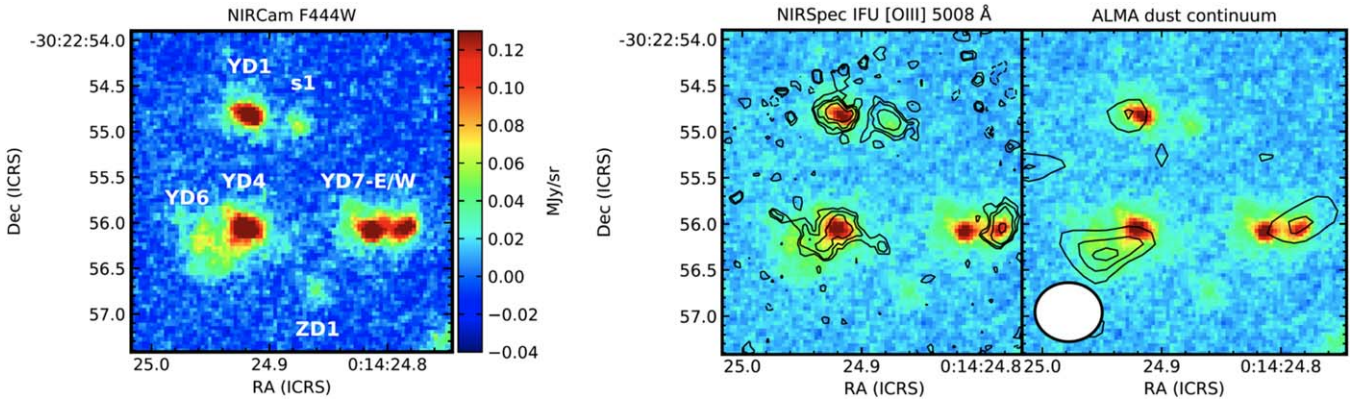


Figure 1. (Left) $3\farcs0 \times 3\farcs0$ cutout image of NIRCam F444W around the "quintet" region. The color bar shows the surface brightness. (Middle) Black contours show the NIRSpec [O III] 5008 Å line map overlaid on the NIRCam F444W image. Contours are drawn at $\pm(2, 3, 4, 5, 6) \times \sigma$, where σ is 1.47 MJy sr^{-1}. (Right) Black contours show the ALMA Band 6 dust continuum map at the rest-frame wavelength $\sim$133 μm overlaid on the F444W image. Contours are drawn at $\pm(2.5, 3.0, 3.3) \times \sigma$, where σ is 6.7 μJy beam^{-1}. The ellipse at the lower left corner indicates the synthesized beam size ($0\farcs73 \times 0\farcs64$).

galaxies at $z = 7.88$ with, e.g., [O III] 4960.295 and 5008.239 Å (hereafter 4960 and 5008 Å), identifying the system as the most distant protocluster reported so far. Observations were made by JWST ERS (program #1324, PI: Treu) and DDT (program #2756, PI: Chen) programs using the NIRSpec (Jakobsen et al. 2022) microshutter array (MSA; Ferruit et al. 2022) mode with a prism ($R \sim 100$) and/or medium-resolution ($R \sim 1000$) configurations.

The combination of JWST NIRSpec integral field spectroscopy (IFS; Böker et al. 2022) and the Atacama Large Millimeter/submillimeter Array (ALMA) is a promising route to identifying member galaxies in a less biased manner and studying their properties such as dust content and star formation history (SFH) in a spatially resolved manner. As part of the JWST GO1 program #1840 (PIs: J. Álvarez-Márquez and T. Hashimoto; Alvarez-Marquez et al. 2021), the Reionization and the ISM/Stellar Origins with JWST and ALMA (RIOJA) project, we are conducting follow-up observations of 12 ALMA [O III] 88 μm emission-line galaxies at $z \sim 6$–8 (e.g., Inoue et al. 2016; Carniani et al. 2017; Laporte et al. 2017; Hashimoto et al. 2019; Harikane et al. 2020; Akins et al. 2022; Sugahara et al. 2022; Witstok et al. 2022) with NIRCam (Rieke et al. 2005; Beichman et al. 2012) and NIRSpec IFS. Here we report observations of the "quintet" galaxy candidates at $z \sim 8$ (Figure 1). Two of the member galaxies (A2744-YD4 and YD7) were already identified in Morishita et al. (2023) at $z = 7.88$. YD4 was also detected in dust continuum emission (Laporte et al. 2017). Throughout this Letter, we assume a set of parameters in ΛCDM cosmology with $\Omega_m = 0.272$, $\Omega_b = 0.045$, $\Omega_\Lambda = 0.728$, and $H_0 = 70.4\,\mathrm{km\,s^{-1}}$ Mpc^{-1} (Komatsu et al. 2011). We adopt the Kroupa initial mass function (Kroupa & Boily 2002). All fluxes are given without correction by magnification factor of $\mu = 2.0$ (Morishita et al. 2023) unless otherwise indicated.

2. JWST Observations of the "Quintet"

2.1. NIRSpec IFS Observations

NIRSpec IFS observations were conducted on 2022 December 16 as part of the JWST GO1 program #1840. The specific observations can be accessed via the Mikulski Archive for Space Telescopes (MAST) at the Space Telescope Science Institute: doi:10.17909/bn0s-2879. The observations were taken with a grating/filter pair of G395H/F290LP that produced a cube with a spectral resolution of $R \sim 2700$ in a wavelength range of 2.87–5.27 μm. A medium size cycling dither pattern of four dithers was used to cover all the quintet galaxies at slightly larger distances than the $3\farcs0 \times 3\farcs0$ IFS field of view. The total exposure time including overhead was 8870 s.

The raw data were processed with the JWST pipeline version 1.11.1 (Bushouse et al. 2022) under CRDS context jwst_1097.pmap. Following the data reduction process used by *Guaranteed* Time Observations programs (e.g., Marshall et al. 2023; Perna et al. 2023; Übler et al. 2023), we applied some modifications to the pipeline including (1) the removal of the $1/f$ noise (c.f., Bagley et al. 2023), (2) rejection of the bad pixels and cosmic rays by sigma-clipping, and (3) removal of a median background in the calibrated images. The data cube was sampled with a pixel size of $0\farcs05$. To set the astrometry in the NIRCam reference system, we cross-correlated the [O III] 5008 Å map with the NIRCam F444W image, the latter significantly contaminated by the [O III] 5008 Å emission.

2.2. NIRCam Observations

NIRCam data were taken as a part of the JWST GO1 program #2561, the UNCOVER survey (PI: Labbe & Bezanson; Labbe et al. 2021). The data include seven filters, F115W, F150W, F200W, F277W, F356W, F410M, and F444W. The data were calibrated with the JWST pipeline version 1.9.4 under CRDS context jwst_1041.pmap. Apart from the standard pipeline stages, we applied custom snowball and wisps correction as described in Bagley et al. (2023). Furthermore, following Pérez-González et al. (2023), a background homogenization algorithm was applied prior to obtaining the final mosaics, all drizzled at a plate scale of $0\farcs03$ px^{-1}. The angular resolution is $\approx 0\farcs14$ in F444W (Figure 1).

We rescaled the photometric errors to take into account the correlated noise introduced by drizzling in the NIRCam images. We used 1000 circular apertures ($r = 0\farcs225$) on blank regions to measured the rms on both the nominal and drizzled images (see also Pérez-González et al. 2023; L. Costantin et al. 2023, in preparation). This effect was estimated to be $\sim$60% for LW bands and 3% on SW bands.

2.3. Identification of Galaxies at z = 7.88

The map of the [O III] 5008 Å line emission integrated over a velocity range of 270 km s^{-1} is overlaid on the NIRCam F444W image in Figure 1 (central panel). The NIRSpec spectra

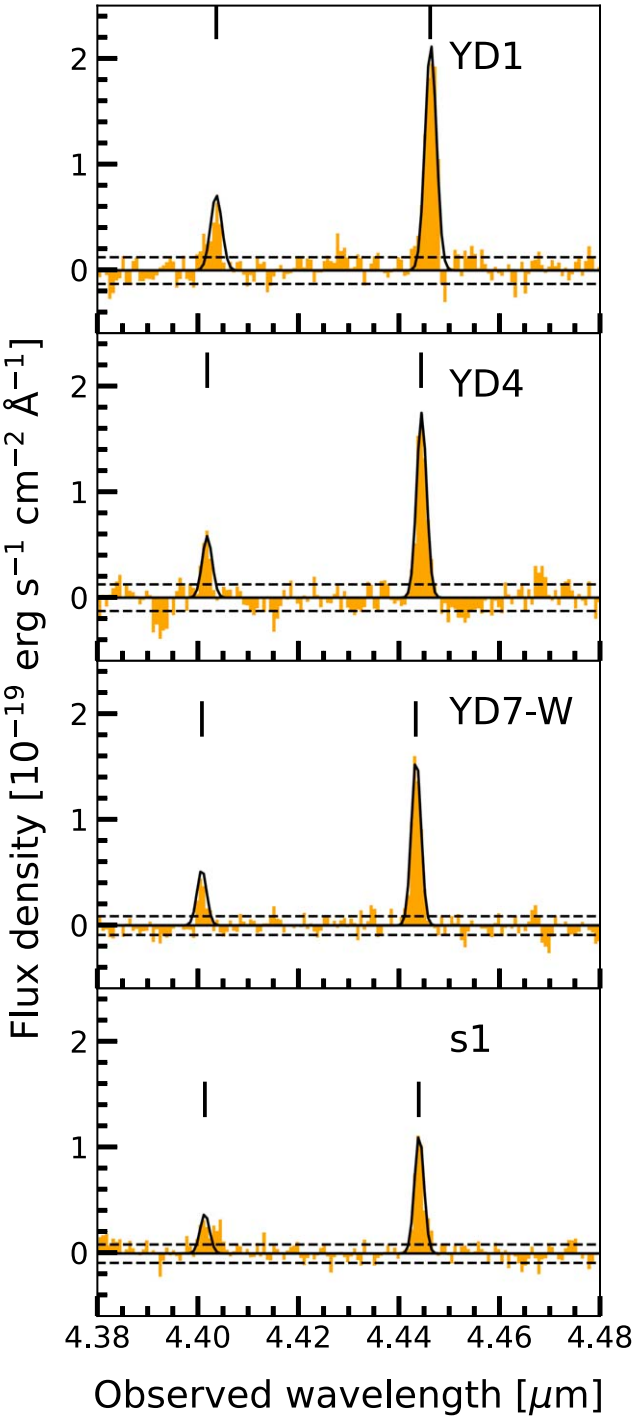


Figure 2. Spectra of [O III] 4960 and 5008 Å associated with A2744-YD1, YD4, the western component of YD7 (YD7-W), and s1. Black solid lines show Gaussian fit results for emission lines, whereas the horizontal dashed lines indicate the typical 1σ uncertainties in the spectra measured around the [O III] 5008 Å lines. The vertical ticks indicate the wavelengths of [O III] 4960 and 5008 Å.

covering the [O III] 4960 and 5008 Å spectral range for the four galaxies with detected [O III] emission are presented in Figure 2. The spectra were spatially integrated over the region corresponding to a 2σ region in the [O III] 5008 Å map, where 1σ is 1.47 MJy sr^{-1}.

In addition to the three known member galaxies, A2744-YD1, YD4, and the western component of YD7 (YD7-W), we serendipitously identified a new galaxy, A2744-s1, that was not recognized as a $z\sim8$ candidate in the previous works based on the HST and Spitzer data. This demonstrates the power of IFS observations to probe the true structure of a protocluster. A2744-ZD1 was not identified in our spectra, which indicates its faint nature in [O III].

Table 1 summarizes the line properties. We measured the spectroscopic redshift, line FWHM, and flux by applying a Gaussian fit to the [O III] 5008 Å lines alone. To obtain uncertainties, we first measured the noise level per spectral bin at $\lambda=4.2$–4.3 and 4.6–4.8 μm, and adopted its standard deviation as the 1σ value. The 1σ value was then considered in the Gaussian fitting. We obtained the spectroscopic redshifts ranging from 7.8721 to 7.8778, corresponding to the maximum velocity offset of 193 ± 10 km s^{-1}. The line FWHM values are measured to be 110–145 km s^{-1} after correction by the instrumental broadening (FWHM$_{\rm inst}=$ 100 km s^{-1}; Jakobsen et al. 2022). In A2744-ZD1, we place a 3σ upper limit on the [O III] 5008 Å flux based on a spectrum extracted from a circular aperture with a radius of 0.″2. In this calculation, we assumed the $z=7.88$ and line FWHM of 150 km s^{-1}. In Figure 2, we also show the Gaussian curves to the [O III] 4960 Å lines, where we adopted the same line FWHMs and redshifts as [O III] 5008 Å, and the peak flux density ratio of 3:1 (Storey & Zeippen 2000).

A2744-YD4 and YD7 were previously observed in Morishita et al. (2023) with the MSA mode. The flux values in Morishita et al. (2023) and those in the present IFS observations are broadly consistent with each other if we take the slit-loss correction factors into account (T. Morishita, private communication).

3. ALMA Dust Continuum Data of A2744-z7p9OD

The spectroscopic identification of the galaxies motivates us to examine dust continuum with ALMA data. The dust continuum was already detected in A2744-YD4 at the significance level of 4σ in ALMA Band 7 data (Laporte et al. 2017). In Appendix A, we reanalyzed the Band 7 data, and present the photometry for the member galaxies. Below, we additionally examine ALMA archival data in Band 6.

The Band 6 data were obtained as a part of an ALMA Cycle 6 program (ID: 2018.1.01332.S, PI: N. Laporte). A single tuning with four spectral windows was used to probe a mean frequency of 254.2 GHz, corresponding to the rest-frame wavelength of 132.8 μm at $z=7.88$.

We reduced and analyzed ALMA data with the default CASA pipeline scripts. We produced a continuum map using all the four spectral windows with a natural weighting to optimize the point-source sensitivity. We adopted the taper value of 0.″4 where the signal-to-noise ratio becomes the highest. The beam size of the tapered map is $0.''73\times0.''64$, and the rms value is 6.7 μJy beam^{-1}.

The right panel of Figure 1 shows the dust continuum contours overlaid on the F444W image. The dust continuum contours show a spatial coincidence in A2744-YD1, YD4, and YD7, within positional uncertainties, at a significance level $>3\sigma$. The continuum flux densities are 83 ± 34, 60 ± 25, and 53 ± 25 μJy in A2744-YD1, YD4, and YD7, respectively, without lensing magnification correction. We note that the spatial resolution of the ALMA Band 6 data is insufficient to spatially resolve A2744-YD4 at $z=7.88$ and YD6 that was reported to be $z=8.38$ (Laporte et al. 2017) with a separation

Table 1
Summary of Properties of the "Quintet" Galaxies

ID	z	$f_{[\mathrm{O\,III}]5008}$ (10^{-18} erg s^{-1} cm^{-2})	FWHM$_{[\mathrm{O\,III}]5008}$ (km s^{-1})	β	M_{UV} (mag)	$\mathrm{A_V}$ (mag)	SFR$_{10\ \mathrm{Myr}}$ ($M_\odot$ yr^{-1})	logM_* ($M_\odot$)	logM_d ($M_\odot$)
YD1	7.8778 ± 0.0001	6.00 ± 0.38	145 ± 9	$-1.25^{+0.11}_{-0.14}$	-18.4 ± 0.1	$0.84^{+0.20}_{-0.25}$	15^{+4}_{-3}	$8.4^{+0.1}_{-0.1}$	6.4
YD4	7.8742 ± 0.0001	4.34 ± 0.36	122 ± 10	$-1.29^{+0.08}_{-0.10}$	-20.2 ± 0.1	$0.65^{+0.13}_{-0.08}$	45^{+10}_{-7}	$9.2^{+0.1}_{-0.1}$	6.5
YD7	7.8721 ± 0.0001	3.78 ± 0.25	113 ± 7	$-1.48^{+0.09}_{-0.10}$	-20.2 ± 0.2	$0.50^{+0.15}_{-0.08}$	31^{+8}_{-5}	$9.1^{+0.1}_{-0.1}$	6.3
s1	7.8732 ± 0.0001	2.63 ± 0.24	110 ± 10	$-1.30^{+0.32}_{-0.32}$	-16.7 ± 0.5	$0.64^{+0.25}_{-0.20}$	3^{+2}_{-1}	$7.6^{+0.3}_{-0.3}$	<5.9
ZD1	7.88[a]	<0.26	N/A	$-1.76^{+0.30}_{-0.23}$	-17.1 ± 0.5	$0.24^{+0.16}_{-0.11}$	$1.0^{+0.6}_{-0.3}$	$8.1^{+0.1}_{-0.1}$	<5.9

Notes. The SED fitting results and dust masses are corrected for the gravitational magnification factor of 2 as measured in Morishita et al. (2023). We calculated SFR from the SFH posterior distributions by averaging star formation rates over 10 Myr. Upper limits are 3σ.
[a] We assumed redshift of $z = 7.88$ for A2744-ZD1 during SED fitting.

of only 0.″45 in the sky coordinate. In Appendix B, we analyzed the positional uncertainty of the Band 6 continuum emission along with the previous Band 7 continuum data of Laporte et al. (2017). These analyses demonstrate that there is a possibility that a part of the Band 6 continuum emission in YD4 could be contaminated by YD6, whereas the Band 7 continuum is likely associated with YD4. In A2744-ZD1 and s1, we place a 3σ upper limit on the flux density to be 20 μJy.

We estimate the total infrared luminosity, L_{IR}, by integrating the modified blackbody radiation over 8–1000 μm.[19] Because dust temperature and emissivity index values cannot be constrained with the current data, we assume a dust temperature of $T_\mathrm{d} = 50$ K and an emissivity index of $\beta_\mathrm{d} = 1.5$ (e.g., Bakx et al. 2021). We obtain $L_{\mathrm{IR}} \approx (1.4 \pm 0.5), (1.6 \pm 0.6)$, and $(0.8 \pm 0.4) \times 10^{11}\ L_\odot$ for A2744-YD1, YD4, and YD7, respectively, after correcting for the cosmic microwave background (CMB) effects (da Cunha et al. 2013). The dust mass is estimated to be $M_\mathrm{d} = (2.7 \pm 1.1)$, (3.3 ± 1.2), and $(1.8 \pm 0.8) \times 10^6\ M_\odot$, for A2744-YD1, YD4, and YD7, respectively, with a dust mass absorption coefficient $\kappa = \kappa_0(\nu/\nu_0)^{\beta_\mathrm{d}}$, where $\kappa_0 = 10\ \mathrm{cm^2\ g^{-1}}$ at 250 μm (Hildebrand 1983). Note that these physical quantities are corrected for the magnification factor of 2.

4. SED Fitting

To obtain physical properties of the galaxies, we performed spectral energy distribution (SED) fitting using photometry obtained from JWST and ALMA observations. We also use the ancillary HST data from the UNCOVER project (Weaver et al. 2023) that include six filters, F435W, F606W, F814W, F125W, F140W, and F160W. Details of our methods are presented in Y. Fudamoto et al. (2023, in preparation), and in the following we summarize essential items.

We used the publicly available SED fitting code BAGPIPES (Carnall et al. 2018) assuming delayed-tau SFH. We adopt a dust attenuation law from Calzetti et al. (2000). For A2744-ZD1, we assume the redshift of $z = 7.88$. The [O III] line and dust continuum fluxes are included in the fitting process, where we correct for the CMB impact on the dust continuum flux densities following da Cunha et al. (2013) and assuming $T_\mathrm{d} = 50$ K. For A2744-s1 and ZD1 in which dust continuum is not detected, the SED fitting uses only the HST and JWST photometry. Then, we checked if the obtained SEDs are consistent with the nondetections of dust continuum. Likewise, for A2744-YD1 and YD7 in which only Band 6 data show the detection, we first run the SED fitting without Band 7 data, and checked if the results are consistent with the nondetections in Band 7.

We obtained reasonable fits as shown in Figure 3. Table 1 summarizes the physical properties. We estimated UV continuum slopes (β), using full SED posteriors by fitting a power-law function in a form of $f_\lambda \propto \lambda^\beta$. The member galaxies have red UV continuum slopes ranging from $\beta = -1.2$ to -1.8, and high stellar dust attenuation ranging from $A_\mathrm{V} = 0.2$ to 0.8 magnitudes, supporting that the member galaxies are relatively dusty and can be classified as luminous infrared galaxies. The present sample has a median A_V/mag value of 0.64 with a standard deviation of 0.20, which is large compared to that of 13 photometrically selected galaxies at $z \sim 7$–9, $A_\mathrm{V}/\mathrm{mag} = 0.20 \pm 0.18$ (Leethochawalit et al. 2023).

The galaxies have stellar masses in the range of $\log(M_*/M_\odot) \sim 7.6$–9.2 and star formation rates (SFRs) of $\sim$3–50 $M_\odot\ \mathrm{yr^{-1}}$, showing a wide variety in stellar properties. We note that the SFR values become twice lower if we adopt a constant SFH.

5. Discussion

5.1. A2744-z7p9OD: An Early z ∼ 8 Protocluster Dust Factory

The "quintet" region demonstrates the accelerated evolution of galaxies. The UV continuum slope is a useful tracer of dust content (e.g., Meurer et al. 1999), and has been systematically investigated in, e.g., Bouwens et al. (2014) and Cullen et al. (2023) at $z \sim 4$–8 and $z \sim 8$–16, respectively. As shown in the bottom right panel of Figure 3, these studies have shown that UV fainter galaxies have smaller β (i.e., bluer) values, indicating that they are less dusty. The red circles indicate the member galaxies, where the UV absolute magnitude, M_{UV}, ranges from -20.2 to -16.7 after the lensing magnification correction (Table 1). The member galaxies show redder β at a given M_{UV}, indicating that they are dustier.

Albeit with large uncertainties in the dust mass estimates due to unknown dust temperature, we roughly estimate the dust-to-stellar mass ratio, $\log(M_\mathrm{d}/M_*)$, to be ≈ -2.0, -2.7, and -2.8 in A2744-YD1, YD4, and YD7, respectively. These are consistent with the median value obtained in a sample of local spiral galaxies (KINGFISH; Kennicutt et al. 2011), $\log(M_\mathrm{d}/M_*) = -3.03^{+0.51}_{-0.78}$ (Calura et al. 2017). The mass ratio is also consistent with the result of semianalytical galaxy formation models of DELPHI (Dayal et al. 2022) that takes into account the Type II supernovae (SNe) dust production, astration, shock destruction, and ejection in outflows.

At $z \sim 8$, a dominant fraction of dust is produced by Type II SNe. Based on the stellar mass estimate and an effective number of SNe per unit stellar mass, $0.15 \times 10^{-2}\ M_\odot^{-1}$

[19] Only in the case of YD4, we use the Band 7 photometry, not Band 6 photometry, due to the potential contamination by YD6 (see Appendix).

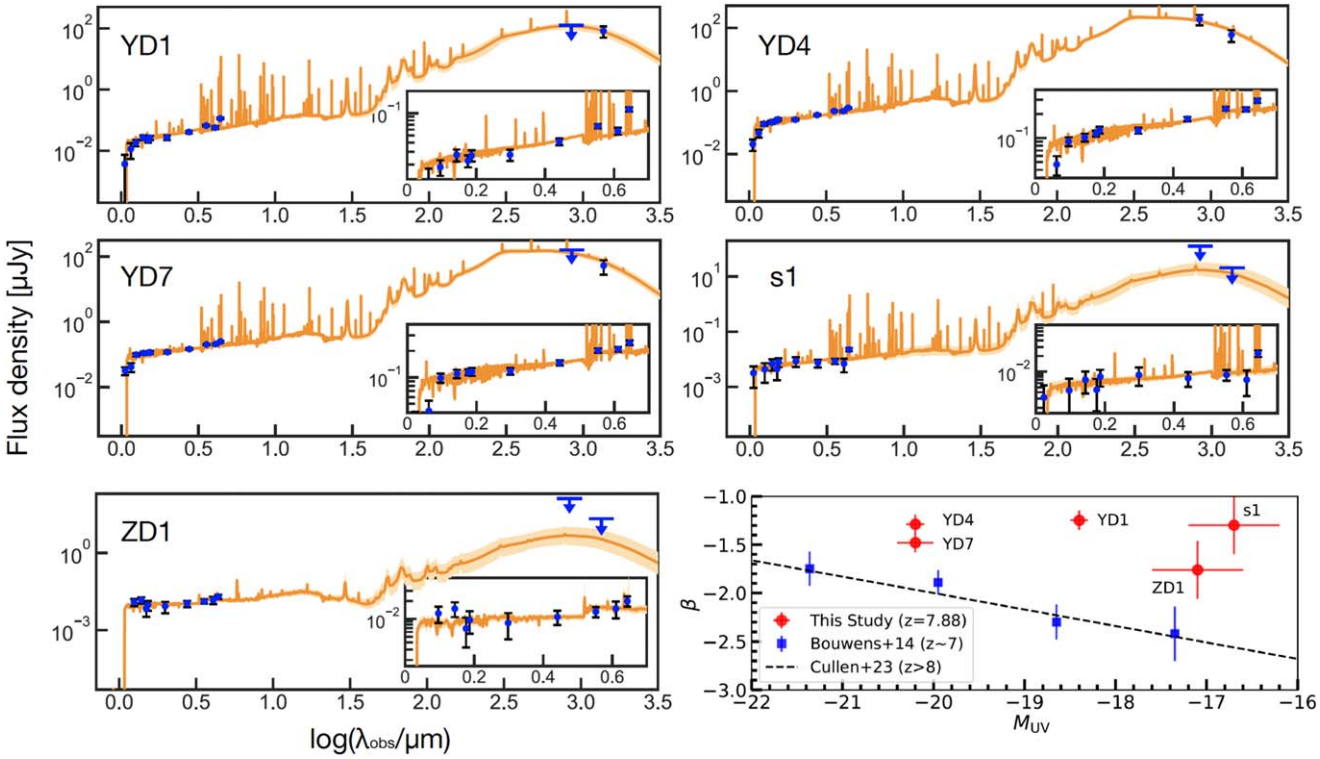


Figure 3. Photometry and results of BAGPIPES SED fitting. Blue points show the aperture photometry using JWST, HST, and ALMA. Downward arrows show 3σ upper limits for ALMA's dust continuum nondetections. Orange solid lines show 50th percentile of the posterior distribution, and the orange bands show 16th to 84th percentile of the posterior distribution. Insets show zoomed in SEDs for the rest-frame UV and optical wavelengths. (Bottom right) The blue squares show the typical observed β as a function of $M_{\rm UV}$ at $z\sim 7$ (Bouwens et al. 2014). The dashed line indicates the best-fit relation between the two quantities at $z>8$ (Cullen et al. 2023). The galaxies in the "quintet" region show redder β (red circles).

(Inoue 2011), we estimate the number of SNe events to be $\approx$(4–20) $\times 10^6$ for the three galaxies. To reproduce the dust mass, we estimate the dust yield per unit SN to be 0.7–1.0 $M_\odot$, which can be reproduced by theoretical models in the case of effective production and inefficient destruction of dust grains (e.g., Leśniewska & Michałowski 2019). Note that the dust yield is reduced if these galaxies have (i) a top-heavy IMF and/or (ii) dust temperature higher than the assumed value of 50 K.

5.2. A2744-z7p9OD: Progenitor Protocluster and Evolution according to FirstLight Simulations

It is interesting to see if an evolved system as the "quintet region" is also found in cosmological simulations. To this end, we use FirstLight simulations (Ceverino et al. 2017), which are a suite of "zoom-in" cosmological simulations with a parsec-scale resolution and provide a larger number of galaxy samples among other simulations (e.g., Pallottini et al. 2017; Katz et al. 2019; Arata et al. 2020). The cosmological box size is 60 comoving Mpc and the maximum spatial resolution is ~9–17 pc, which are well suited to study the internal structure of rare objects such as the "quintet."

We have successfully found an analog of the "quintet" region. Panel (a) of Figure 4 shows the density projection of the simulation sample, FL957, at $z=7.7$. There are four galaxies within a $3''\times 3''$ region, and there is yet another stellar clump within $\sim 1\farcs5$ (~5 kpc). The stellar masses of the four clustered galaxies are $M_*=4.2$, 5.8, 8.6, and 7.2×10^8 $M_\odot$, consistent with the observed values within a factor of 2 (Table 1). The maximum velocity offset among the four simulated clumps is 131 km s^{-1}, similar to the observed value of 193 ± 10 km s^{-1}. We calculate the [O III] 5008 Å luminosity in the same manner as in Nakazato et al. (2023). Panel (b) of Figure 4 shows the [O III] 5008 Å line surface brightness, where we assume dust extinction of $A_{5008}=0.25$ mag following the relation between stellar mass and attenuation as reported in Mushtaq et al. (2023) for FirstLight simulation. The total line luminosity in the region is 1.95×10^{43} erg s^{-1}, which is consistent with the total intrinsic luminosity of the observed galaxies, 0.62×10^{43} erg s^{-1}, within a factor of 3. Finally, assuming a fixed dust-to-metal ratio of 0.4, the dust-to-stellar mass ratio is log $(M_{\rm d}/M_*)\sim -2.5$, again consistent with the observed values.

The simulations allow us to follow the further evolution of the system. We find that galaxy 2 and 3 merge at $z=7.5$ (panel (c)), and finally become a massive galaxy with $M_*=5.47\times 10^9$ $M_\odot$ at $z=7.3$ (panel (d)). The rapid evolution implies that the "quintet" galaxies are likely on the verge of merging in a few to several tens of Myr. Detailed SFH and gas dynamics will be studied in our forthcoming paper (Y. Nakazato et al. 2023, in preparation).

6. Conclusions

We have presented the JWST NIRSpec IFS observations of the core of the most distant protocluster at $z=7.88$, A2744-z7p9OD.

1. We have identified four galaxies at $z=7.88$ with [O III] 4960 and 5008 Å within a $\sim 11\times 11$ kpc region. The galaxies have a small velocity offset of 193 ± 10 km s^{-1}, suggesting a close association of these galaxies.

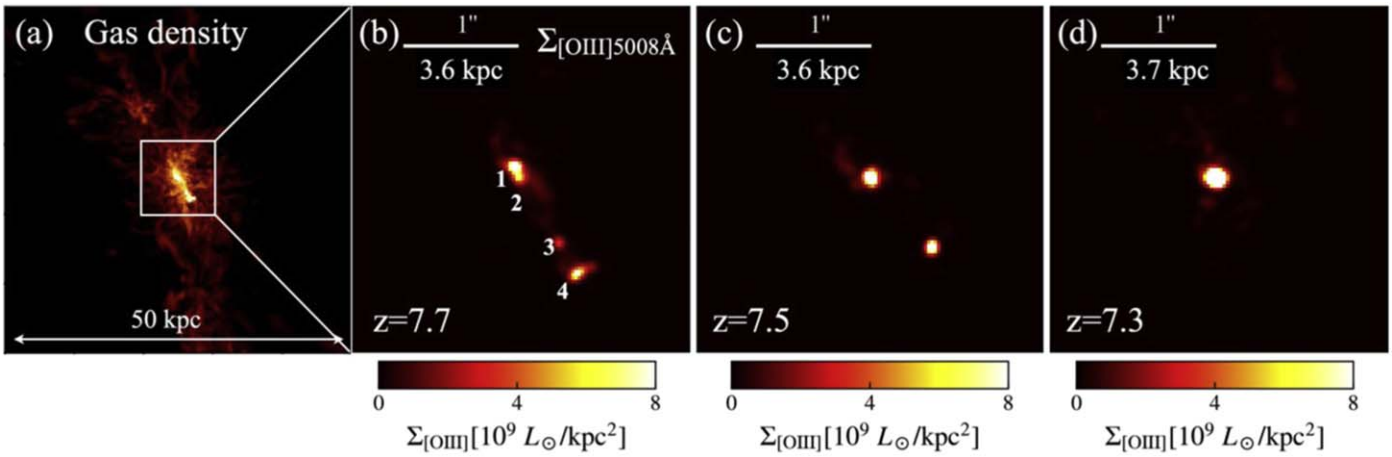


Figure 4. Projected gas density (panel (a)) and [O III] 5008 Å distribution (panel (b)) for a galaxy sample FL957 (Ceverino et al. 2017) at $z = 7.7$. Each panel shows a region with a side length and depth of 50 and 10.6 kpc, the latter corresponds to the NIRSpec IFS field of 3″ with magnification of $\mu \sim 2$. Panels (c) and (d) show the following evolution of FL957 at $z = 7.5$ and 7.3, demonstrating that the system finally becomes a large massive galaxy by $z = 7.3$.

2. ALMA Band 6 dust continuum data show 3σ signals at the positions of A2744-YD1, YD4+YD6, and YD7, whereas Band 7 data show 4σ signal at the position of YD4. Assuming a dust temperature of 50 K and an emissivity index of 1.5, these three galaxies have $L_{IR} \sim 10^{11} L_\odot$ and $M_d \sim (1\text{–}3) \times 10^6 M_\odot$.
3. The presence of dust is consistent with their red UV continuum slopes, $\beta \sim -1.3$. The galaxies have redder β values at a given M_{UV} compared to typical $z \gtrsim 7$ galaxies.
4. With the BAGPIPES SED fitting code assuming delayed-tau SFH, the member galaxies have stellar masses in the range of $\log(M_*/M_\odot) \sim 7.6\text{–}9.2$ and SFRs of $\sim 3\text{–}50\ M_\odot\ yr^{-1}$, showing a diversity in their properties.
5. Following FirstLight cosmological simulations reproducing the observed physical properties of the member galaxies, the expected evolution of the core protocluster is to form a larger, massive galaxy with a stellar mass of $M_* \sim 6 \times 10^9 M_\odot$ at $z \sim 7.3$.

The present study demonstrates the power of JWST NIRSpec IFS observations to probe the true structure of a protocluster. The presence of a multiple merger and evolved galaxies in the core region of A2744-z7p9OD indicates that environmental effects are already at work 650 Myr after the Big Bang.

Acknowledgments

We thank an anonymous referee for valuable comments that have greatly improved the paper. This paper makes use of the following ALMA data: ADS/JAO.ALMA #2015.1.00594S and #2018.1.01332.S. ALMA is a partnership of ESO (representing its member states), NSF (USA), and NINS (Japan), together with NRC (Canada), NSC and ASIAA (Taiwan), and KASI (Republic of Korea), in cooperation with the Republic of Chile. The Joint ALMA Observatory is operated by ESO, AUI/NRAO, and NAOJ. This work has made use of data from the European Space Agency (ESA) mission Gaia (https://www.cosmos.esa.int/gaia), processed by the Gaia Data Processing and Analysis Consortium (DPAC, https://www.cosmos.esa.int/web/gaia/dpac/consortium). Funding for the DPAC has been provided by national institutions, in particular the institutions participating in the Gaia Multilateral Agreement. T.H. was supported by Leading Initiative for Excellent Young Researchers, MEXT, Japan (HJH02007) and by JSPS KAKENHI grant No. 22H01258. A.K.I., Y.S., and Y.F. are supported by NAOJ ALMA Scientific Research grant No. 2020-16B. A.K.I. also acknowledges funding from JSPS KAKENHI grant No. 23H00131. Y.T. is supported by JSPS KAKENHI grant No. 22H04939. K.M. acknowledges financial support from the Japan Society for the Promotion of Science (JSPS) through KAKENHI grant No. 20K14516. J. A.-M., L.C., A.C-G., and C.B.-P. acknowledge support by grant PIB2021-127718NB-100 from the Spanish Ministry of Science and Innovation/State Agency of Research MCIN/AEI/10.13039/501100011033 and by "ERDF A way of making Europe". C.B.-P. acknowledges support by grant CM21_CAB_M2_01 from the Program "Garantía Juveníl" from the "Comunidad de Madrid" 2021. L.C. acknowledges financial support from Comunidad de Madrid under Atracción de Talento grant 2018-T2/TIC-11612. M.P.S. acknowledges funding support from the Ramón y Cajal program of the Spanish Ministerio de Ciencia e Innovación (RYC2021-033094-I). We are grateful to Takahiro Morishita, Nicolas Laporte, Guido Roberts-Borsani, Seiji Fujimoto, and Hide Yajima for useful discussion.

Facilities: JWST (STIS), ALMA.

Software: astropy (Astropy Collaboration et al. 2022), photoutils (Bradley et al. 2022), BAGPIPE (Carnall et al. 2018), CLOUDY (Ferland et al. 2017).

Appendix A
ALMA Band 7 Data

We have reanalyzed the archival ALMA Band 7 data (ID: 2015.1.00594S, PI: N. Laporte). The data probe a mean frequency of 356.0 GHz, corresponding to the rest-frame wavelength of 94.8 μm at $z = 7.88$. The continuum image has an rms level of 23.4 μJy per beam at the phase center of (α_{ICRS}, δ_{ICRS}) = ($00^h14^m25\overset{s}{.}081$, $-30°22'49\overset{''}{.}70$), with a beam size of $0\overset{''}{.}25 \times 0\overset{''}{.}18$. Because the core region of A2744-z7p9OD is $\sim 7''$ away from the phase center, we need to correct for the the primary beam attenuation. With a correction factor of 0.65, the effective rms level of the continuum image is 36.1 μJy per beam. The continuum image reveals a 4σ detection at the position of (α_{ICRS}, δ_{ICRS}) = ($00^h14^m24\overset{s}{.}939$, $-30°22'56\overset{''}{.}06$). With a

positional uncertainty of $\approx 0\farcs06$ (see Equation (10.7) of the ALMA Cycle 10 Technical Handbook), this signal is likely associated with YD4, as first reported by Laporte et al. (2017). The flux density is estimated to be 189 ± 68 μJy, which is larger than the previous measurement in Laporte et al. (2017) due to the primary beam attenuation correction. Other member galaxies at $z \sim 7.88$ (YD1, YD7, ZD1, s1) and YD6 at $z = 8.38$ are not detected above 3σ. With the 3σ upper limit of the brightness, 108 μJy per beam, and integrating over the size of these galaxies, the 3σ upper limits on the flux densities are 127, 127, 160, and 127 μJy for A2744-YD1, YD6, YD7, s1, and ZD1, respectively. Note that these values are not corrected for the magnification factor of 2.

Appendix B
Astrometry of ALMA Band 6 Data

The peak positions of the ALMA Band 6 dust continuum emission for A2744-YD1, YD4+YD6, and YD7 are ($\alpha_{\rm ICRS}$, $\delta_{\rm ICRS}$) = ($00^{\rm h}14^{\rm m}24\fs930$, $-30°22'54\farcs79$), ($00^{\rm h}14^{\rm m}24\fs945$, $-30°22'56\farcs35$), ($00^{\rm h}14^{\rm m}24\fs791$, $-30°22'55\farcs98$), respectively. With the peak significance levels of 3.0σ (YD1), 3.3σ (YD4+YD6), and 3.1σ (YD7), and the beam size of the image ($0\farcs73 \times 0\farcs64$), the positional uncertainties of the dust continuum emission are $\approx 0\farcs25$. This indicates that the Band 6 dust continuum around YD4 could be contaminated by YD6.

Appendix C
NIRspec IFS Result of A2744-YD6

Laporte et al. (2017) originally reported 4σ detections of [O III] 88 μm and Lyα with ALMA and VLT/X-Shooter, respectively, at $z = 8.38$ from YD4 (see also Carniani et al. 2020). However, the redshift of YD4 is updated to be $z = 7.88$ by Morishita et al. (2023), as reproduced by our IFS observations. The authors discussed the possibility that the source detected at $z = 8.38$ is in the background of the protocluster at $z = 7.88$, and likely associated with YD6, whereas the dust continuum detection is likely associated with YD4 (see Figure 2 in Laporte et al. 2019). We examined the presence of an emission line at the position of A2744-YD6; however, our NIRSpec IFS data do not show any optical emission lines such as Hβ or [O III] at $z = 8.38$. Assuming a line FWHM of 100 km s^{-1}, the 3σ upper limit for the [O III] 5008 Å line is 0.23×10^{-18} erg s^{-1} cm^{-2} for YD6. Future deeper JWST observations are crucial for confirming whether YD6 is at $z = 8.38$ using optical emission lines.

ORCID iDs

T. Hashimoto https://orcid.org/0000-0002-0898-4038
J. Álvarez-Márquez https://orcid.org/0000-0002-7093-1877
Y. Fudamoto https://orcid.org/0000-0001-7440-8832
L. Colina https://orcid.org/0000-0002-9090-4227
A. K. Inoue https://orcid.org/0000-0002-7779-8677
Y. Nakazato https://orcid.org/0000-0002-0984-7713
D. Ceverino https://orcid.org/0000-0002-8680-248X
N. Yoshida https://orcid.org/0000-0001-7925-238X
L. Costantin https://orcid.org/0000-0001-6820-0015
Y. Sugahara https://orcid.org/0000-0001-6958-7856
A. Crespo Gómez https://orcid.org/0000-0003-2119-277X
C. Blanco-Prieto https://orcid.org/0009-0005-5448-5239
K. Mawatari https://orcid.org/0000-0003-4985-0201
S. Arribas https://orcid.org/0000-0001-7997-1640
R. Marques-Chaves https://orcid.org/0000-0001-8442-1846
M. Pereira-Santaella https://orcid.org/0000-0002-4005-9619
T. J. L. C. Bakx https://orcid.org/0000-0002-5268-2221
M. Hagimoto https://orcid.org/0000-0001-8083-5814
H. Matsuo https://orcid.org/0000-0003-3278-2484
Y. Tamura https://orcid.org/0000-0003-4807-8117

References

Akins, H. B., Fujimoto, S., Finlator, K., et al. 2022, ApJ, 934, 64
Alvarez-Marquez, J., Hashimoto, T., Arribas, S., et al. 2021, ALMA [OIII] 88um Emitters. Signpost of Early Stellar Buildup and Reionization in the Universe, JWST Proposal. Cycle 1, ID. #1840
Arata, S., Yajima, H., Nagamine, K., Abe, M., & Khochfar, S. 2020, MNRAS, 498, 5541
Astropy Collaboration, Price-Whelan, A. M., Lim, P. L., et al. 2022, ApJ, 935, 167
Bagley, M. B., Finkelstein, S. L., Koekemoer, A. M., et al. 2023, ApJL, 946, L12
Bakx, T. J. L. C., Sommovigo, L., Carniani, S., et al. 2021, MNRAS, 508, L58
Beichman, C. A., Rieke, M., Eisenstein, D., et al. 2012, Proc. SPIE, 8442, 84422N
Böker, T., Arribas, S., Lützgendorf, N., et al. 2022, A&A, 661, A82
Bouwens, R. J., Illingworth, G. D., Oesch, P. A., et al. 2014, ApJ, 793, 115
Bradley, L., Sipőcz, B., Robitaille, T., et al. 2022, astropy/photutils: v1.5.0, Zenodo, doi:10.5281/zenodo.6825092
Bunker, A. J., Saxena, A., Cameron, A. J., et al. 2023, arXiv:2302.07256
Bushouse, H., Eisenhamer, J., Dencheva, N., et al. 2022, spacetelescope/jwst: JWST v1.6.2, Zenodo, doi:10.5281/zenodo.6984366
Calura, F., Pozzi, F., Cresci, G., et al. 2017, MNRAS, 465, 54
Calzetti, D., Armus, L., Bohlin, R. C., et al. 2000, ApJ, 533, 682
Carnall, A. C., McLure, R. J., Dunlop, J. S., & Davé, R. 2018, MNRAS, 480, 4379
Carniani, S., Ferrara, A., Maiolino, R., et al. 2020, MNRAS, 499, 5136
Carniani, S., Maiolino, R., Pallottini, A., et al. 2017, A&A, 605, A42
Ceverino, D., Glover, S. C. O., & Klessen, R. S. 2017, MNRAS, 470, 2791
Cullen, F., McLure, R. J., McLeod, D. J., et al. 2023, MNRAS, 520, 14
Curtis-Lake, E., Carniani, S., Cameron, A., et al. 2023, NatAs, 7, 622
da Cunha, E., Groves, B., Walter, F., et al. 2013, ApJ, 766, 13
Dayal, P., Ferrara, A., Sommovigo, L., et al. 2022, MNRAS, 512, 989
Dressler, A. 1980, ApJ, 236, 351
Ferland, G. J., Chatzikos, M., Guzmán, F., et al. 2017, RMxAA, 53, 385
Ferruit, P., Jakobsen, P., Giardino, G., et al. 2022, A&A, 661, A81
Gardner, J. P., Mather, J. C., Abbott, R., et al. 2023, arXiv:2304.04869
Harikane, Y., Ouchi, M., Inoue, A. K., et al. 2020, ApJ, 896, 93
Hashimoto, T., Inoue, A. K., Mawatari, K., et al. 2019, PASJ, 71, 71
Hildebrand, R. H. 1983, QJRAS, 24, 267
Inoue, A. K. 2011, EP&S, 63, 1027
Inoue, A. K., Tamura, Y., Matsuo, H., et al. 2016, Sci, 352, 1559
Ishigaki, M., Ouchi, M., & Harikane, Y. 2016, ApJ, 822, 5
Jakobsen, P., Ferruit, P., Alves de Oliveira, C., et al. 2022, A&A, 661, A80
Katz, H., Galligan, T. P., Kimm, T., et al. 2019, MNRAS, 487, 5902
Kennicutt, R. C., Calzetti, D., Aniano, G., et al. 2011, PASP, 123, 1347
Komatsu, E., Smith, K. M., Dunkley, J., et al. 2011, ApJS, 192, 18
Koyama, Y., Kodama, T., Shimasaku, K., et al. 2008, MNRAS, 391, 1758
Kroupa, P., & Boily, C. M. 2002, MNRAS, 336, 1188
Labbe, I., Bezanson, R., Atek, H., et al. 2021, UNCOVER: Ultra-deep NIRCam and NIRSpec Observations Before the Epoch of Reionization, JWST Proposal. Cycle 1, ID. #2561
Laporte, N., Ellis, R. S., Boone, F., et al. 2017, ApJL, 837, L21
Laporte, N., Katz, H., Ellis, R. S., et al. 2019, MNRAS, 487, L81
Laporte, N., Streblyanska, A., Clement, B., et al. 2014, A&A, 562, L8
Leethochawalit, N., Trenti, M., Santini, P., et al. 2023, ApJL, 942, L26
Leśniewska, A., & Michałowski, M. J. 2019, A&A, 624, L13
Marshall, M. A., Perna, M., Willott, C. J., et al. 2023, arXiv:2302.04795
Meurer, G. R., Heckman, T. M., & Calzetti, D. 1999, ApJ, 521, 64
Morishita, T., Roberts-Borsani, G., Treu, T., et al. 2023, ApJL, 947, L24
Mushtaq, M., Ceverino, D., Klessen, R. S., Reissl, S., & Puttasiddappa, P. H. 2023, MNRAS, Advance Access
Nakazato, Y., Yoshida, N., & Ceverino, D. 2023, ApJ, 952, 140
Pallottini, A., Ferrara, A., Gallerani, S., et al. 2017, MNRAS, 465, 2540
Pérez-González, P. G., Costantin, L., Langeroodi, D., et al. 2023, ApJL, 951, L1

Perna, M., Arribas, S., Marshall, M., et al. 2023, arXiv:2304.06756
Rieke, M. J., Kelly, D., & Horner, S. 2005, Proc. SPIE, 5904, 1
Storey, P. J., & Zeippen, C. J. 2000, MNRAS, 312, 813
Sugahara, Y., Inoue, A. K., Fudamoto, Y., et al. 2022, ApJ, 935, 119
Übler, H., Maiolino, R., Curtis-Lake, E., et al. 2023, arXiv:2302.06647
Weaver, J. R., Cutler, S. E., Pan, R., et al. 2023, arXiv:2301.02671
Witstok, J., Smit, R., Maiolino, R., et al. 2022, MNRAS, 515, 1751
Zheng, W., Shu, X., Moustakas, J., et al. 2014, ApJ, 795, 93